7512–7521 Nucleic Acids Research, 2013, Vol. 41, No. 15 Published online 13 June 2013
doi:10.1093/nar/gkt510

Two RNA-binding motifs in eIF3 direct HCV IRES-dependent translation

Chaomin Sun[1], Jordi Querol-Audí[1], Stefanie A. Mortimer[1], Ernesto Arias-Palomo[1], Jennifer A. Doudna[1,2,3], Eva Nogales[1,3,4] and Jamie H. D. Cate[1,2,5,*]

[1]Department of Molecular and Cell Biology, University of California, Berkeley, CA 94720, USA, [2]Physical Biosciences Division, Lawrence Berkeley National Laboratory, Berkeley, CA 94720, USA, [3]Howard Hughes Medical Institute, University of California, Berkeley, CA 94720, USA, [4]Life Sciences Division, Lawrence Berkeley National Laboratory, Berkeley, CA 94720, USA and [5]Department of Chemistry, University of California, Berkeley, CA 94720, USA

Received March 22, 2013; Revised April 26, 2013; Accepted May 1, 2013

ABSTRACT

The initiation of protein synthesis plays an essential regulatory role in human biology. At the center of the initiation pathway, the 13-subunit eukaryotic translation initiation factor 3 (eIF3) controls access of other initiation factors and mRNA to the ribosome by unknown mechanisms. Using electron microscopy (EM), bioinformatics and biochemical experiments, we identify two highly conserved RNA-binding motifs in eIF3 that direct translation initiation from the hepatitis C virus internal ribosome entry site (HCV IRES) RNA. Mutations in the RNA-binding motif of subunit eIF3a weaken eIF3 binding to the HCV IRES and the 40S ribosomal subunit, thereby suppressing eIF2-dependent recognition of the start codon. Mutations in the eIF3c RNA-binding motif also reduce 40S ribosomal subunit binding to eIF3, and inhibit eIF5B-dependent steps downstream of start codon recognition. These results provide the first connection between the structure of the central translation initiation factor eIF3 and recognition of the HCV genomic RNA start codon, molecular interactions that likely extend to the human transcriptome.

INTRODUCTION

The initiation of eukaryotic protein synthesis is one of the most highly regulated steps in gene expression. Cap-dependent translation requires ≥12 initiation factors (eIFs) to associate with the 7-methyl guanosine cap at the 5′ end of mRNA and the 40S ribosomal subunit, leading to the formation of a 43S preinitiation complex that scans to the correct initiation codon and positions the initiating methionyl-tRNA (Met-tRNAi). The resulting 48S preinitiation complex then associates with the 60S ribosomal subunit to form an active 80S ribosome (1–3). In viruses such as hepatitis C virus (HCV), structured RNA sequences called internal ribosome entry sites (IRESs) located in the genomic 5′-untranslated region trigger an alternative cap-independent mechanism of assembling the eukaryotic protein synthesis machinery at the correct start codon (3,4). The HCV IRES drives translation of its genomic RNA, helping the virus to evade the host immune response that suppresses canonical cap-dependent translation (4). However, the specific molecular events that accompany preinitiation complex formation in an mRNA cap- or IRES-dependent manner remain poorly understood.

Translation initiation factor eIF3 is central to the assembly of competent translation preinitiation complexes (3). Evidence now indicates that eIF3 stimulates most of the reactions in cap-dependent translation initiation, including initiation factor binding to the 40S subunit in the 43S preinitiation complex, mRNA recruitment to the 43S preinitiation complex, mRNA scanning for the start codon (2) and release of eIF2–guanosine diphosphate (GDP) after start codon recognition (5). Human eIF3 also extends the length of the mRNA-binding channel of the 40S subunit in initiation complexes (6). In humans, eIF3 is important for cell homeostasis, and misregulation of eIF3 subunit expression correlates with cancer progression (7). In addition, human eIF3 plays an important role in translation initiation mediated by the HCV IRES. Defined secondary and tertiary structural elements of the HCV IRES (8) bind specifically to eIF3 and the 40S ribosomal subunit (4,9–11). These structural interactions position the genomic RNA at the correct start codon without the need for the 5′-cap binding translation

*To whom correspondence should be addressed. Tel: +1 510 666 2749; Fax: +1 510 643 0080; Email: jcate@lbl.gov
Present address:
Jordi Querol-Audi, Molecular Biology Institute of Barcelona (IBMB-CSIC), Parc Científic de Barcelona, Baldiri i Reixac 10, 08028-Barcelona, Spain.

initiation machinery and mRNA scanning (12,13). HCV IRES–eIF3 association has been proposed to substitute for translation initiation factor eIF4G, which is required for cap-dependent translation (14). However, the molecular consequences of HCV IRES interactions with eIF3 are unknown.

Despite the biological significance of eIF3, its molecular contributions to translation initiation remain unclear owing to the scarcity of structural information. Human eIF3 is an 800 kDa complex containing 13 proteins (eIF3a–eIF3m) (15). The cryo-electron microscopic reconstruction of endogenously purified human eIF3 revealed a five-lobed structure with anthropomorphic features that binds to the platform of the 40S ribosomal subunit (14). Remarkably, our recent 3D reconstruction of a bacterially reconstituted octameric core complex of eIF3 showed it to be structurally similar to the larger native eIF3, likely due to the inherent flexibility of large regions within the complex beyond the central core (16).

In the case of HCV IRES-mediated translation, cryo-EM reconstructions of the binary HCV IRES–eIF3 complex revealed extensive interactions between the IRES RNA and eIF3. However, the specific regions of contact could not be identified definitively (14). In cross-linking experiments, eIF3 subunits a, b, d and f were shown to be located near to or contacting the HCV IRES (10,17). The functional importance of these interactions remains obscure owing to the paucity of structural information about them.

Here we used EM, biochemical and bioinformatics approaches to determine the critical domains responsible for eIF3 binding to the HCV IRES and 40S ribosomal subunit, and for the formation of translation initiation complexes. Together, these results provide fundamental mechanistic insights into eIF3 function during HCV IRES-mediated translation, identify possible new targets for HCV therapeutic intervention and reveal motifs in eIF3 that may be important for the control of translation initiation on cellular mRNAs.

MATERIALS AND METHODS

In vitro reconstitution of eIF3 subcomplexes

All the transfer and coexpression vectors used for generating eIF3 subcomplexes are listed in Supplementary Tables S1 and S2. Quikchange mutagenesis (Agilent Technologies) was used to mutate the predicted helix-loop-helix (HLH) motifs in subunits a and c. Expression and purification of eIF3 subcomplexes are described in the Supplementary Materials and Methods.

Purification of eIF3, 40S ribosomal subunits and HCV IRES RNAs

Human eIF3 and 40S ribosomal subunits, the HCV IRES and IIIabc domains were purified as described (18). The sequence of the IRES IIIabc domain is that used previously (18). The IRES used in rabbit reticulocyte lysate (RRL) initiation complex formation includes nucleotides 39–352 of the HCV subtype 1 b genomic RNA (16). The HCV IRES and IIIabc domain were labeled at the 3′ end for use in native gel mobility shift assays, as described (16).

Reconstituted eIF3 interactions with the HCV IRES, IIIabc domain and 40S ribosomal subunit

Binding reactions to the HCV IRES or IIIabc domain contained reconstituted human eIF3 (or eIF3 subcomplex), labeled HCV IRES or IIIabc domain at 20 nM and THEMK buffer (34 mM Tris, 66 mM HEPES, 0.1 mM EDTA, 2.5 mM $MgCl_2$, 75 mM KCl, pH 7.8). Reactions were carried out at 25°C for 15 min and then resolved by native 1% agarose gels at 4°C for 45 min in the same buffer (18). Gels were visualized by fluorescence imaging using a Typhoon Scanner (Amersham Biosciences). The excitation and emission wavelengths to detect the HCV IRES were 494 and 518 nm, respectively. Binding reactions with the 40S ribosomal subunit were carried out at 25°C for 15 min in ribosome binding buffer (20 mM Hepes, pH 7.5, 100 mM KCl, 2.5 mM $MgCl_2$). Native agarose gel electrophoresis used to monitor binding was carried out at 4°C in THEMK buffer with frequent buffer exchanges.

SHAPE modification chemistry

The full-length IRES within the context of 5′ and 3′ flanking sequences were transcribed, purified and annealed as described in the Supplementary Materials and Methods (19). Folded RNA samples were placed at room temperature for 10 min before reaction with 1-methyl-7-nitroisatoic anhydride (1M7) (20). The folded RNA was incubated with the eIF3 subcomplexes or eIF3 storage buffer at room temperature for 10 min before reaction with 1M7. The eIF3 subcomplexes were in 1.5-fold excess over IRES RNA, at concentrations >250-fold the K_d of the interaction to ensure binding (9). SHAPE modification, reverse transcription, capillary electrophoresis and data processing and normalization were performed as previously described (19) with minor modifications (Supplementary Materials and Methods).

In vitro translation assays with reconstituted eIF3 or its mutants

The *in vitro* translation assays were carried out as described (16). To check the formation of preinitiation complexes, 2 mM 5′-Guanylyl imidodiphosphate (GMPPNP) (Sigma) was added to the reactions. The reactions were run on 10–25% sucrose gradients as described (16). To check the formation of 80S complexes, 100 μg/ml cycloheximide (Sigma) was added to the reactions. The reactions were run on 10–40% sucrose gradient as described (16). The DNA oligonucleotide 5′-AACGATCAGAGTAGTGGT ATTTCACC-3′ was used as the probe for detecting human 28S rRNA (21). All the western blots and northern blots were carried out as described in (16).

Cryo-electron microscopy

C-flat 400-mesh grids containing 2 μm holes with a spacing of 2 μm (Protochips) were glow-discharged in a nitrogen atmosphere for 45 s using an Edwards Carbon

Evaporator. Grids were immediately loaded into a Vitrobot (FEI company) whose climate chamber had equilibrated to 4°C and 100% humidity. Four microliters of aliquots of the purified sample were placed onto the grids. The grids were blotted for 3.5 s at an offset of −1 mm, and plunged into liquid ethane. Because certain views of the eIF3 core particle were missing for the samples using holey grids, the purified complex was also frozen using grids onto which a thin carbon film was floated. Data were acquired on a Gatan 4 K × 4 K camera using a Tecnai F20 electron microscope operating at 120 keV at a nominal magnification of 100 000× using a dose of ~20 $e^-/Å^2$ and a defocus range from −1.2 to −2.5 μm.

Image processing

Data processing (2D) was performed using programs and utilities contained within the Appion processing environment (22). After some initial preprocessing, particle image stacks were subjected to several rounds of reference-free 2D classification by iterative multivariate statistical analysis and multireference alignment using IMAGIC (23). The cryo-EM reconstructions were performed using either an iterative projection matching approach in EMAN2 (24,25) or a maximum-likelihood approach (26) within the XMIPP package (27). We used as an initial reference the negative-stain structure of the human eIF3 core we previously solved (16), filtered to 60 Å resolution. More details can be found in the Supplementary Materials and Methods.

RESULTS

Subunits eIF3a and eIF3c recruit the HCV IRES to the eIF3 octameric core

A prior cryo-EM reconstruction showed the HCV IRES extending across eIF3, from the left arm to the right leg (11,14). In that study, the IRES IIIabc domain was modeled near the right leg of eIF3. However, independent corroborating evidence for the positioning of domains within the HCV IRES in the ternary complex with eIF3 and the 40S ribosomal subunit is lacking. The octameric core of eIF3 binds to the HCV IRES or IIIabc domain RNA (Figure 1A) with an affinity similar to that of native eIF3 (16). We therefore collected cryo-EM data for the eIF3 octameric core bound to the IRES IIIabc domain to better orient the IRES RNA when bound to eIF3 (Supplementary Materials and Methods). Although conformational flexibility and substoichometric binding (Supplementary Figure S1) hampered 3D reconstructions of the eIF3 core/IIIabc RNA complex at high resolution, a multimodel refinement approach (26) yielded one 3D reconstruction with clear extra density, when compared with the unbound eIF3 core, which emanates from the left arm of eIF3, the position of the N-terminus of eIF3a (28) (Figure 1A and Supplementary Figure S1C). The presence of this extra density was confirmed in 3D difference maps (Figure 1A) and agreed with the conclusions from reference-free 2D class average analysis (Supplementary Figure S1). Recent EM labeling experiments have shown this region in the eIF3 core structure to be occupied by subunits a and c (28). Interestingly, limited proteolysis and UV cross-linking experiments revealed that eIF3 subunits a* and c* (the N-terminally truncated versions of eIF3a and eIF3c used in the octameric core reconstitution) become protected by binding of the IIIabc domain RNA, and that they form cross-links with 4-thio-U substituted HCV IRES RNA (Supplementary Figure S2A–2C; Supplementary Materials and Methods). Taken together, these results reveal that the IIIabc domain of the HCV IRES is positioned near the left arm of eIF3 where it interacts with eIF3 subunits a* and c*, and not by the right leg (14).

Conserved residues in eIF3 subunits a and c control HCV IRES binding

To determine the regions of eIF3 subunits a and c that bind the HCV IRES IIIabc domain, the sequences of these two subunits were analyzed computationally with BindN (29) and Phyre^2 (30).These analyses predicted the presence of RNA-binding HLH motifs near amino acid 40 of subunit a and 340 of subunit c, both near the N-termini of the a* and c* truncated subunits used in the eIF3 reconstitution (Figure 1B). The predicted HLH motif in subunit c is highly conserved in all eukaryotic eIF3s, and that in subunit a is highly conserved in metazoans (Figure 1C, Supplementary Figure S2D). Notably, an N-terminal deletion in subunit a* (residues 5–46) that includes its predicted HLH motif reduced the apparent binding of the eIF3 octamer to the HCV IRES over 30-fold (Figure 2A). Further deletion of amino acids 302–343 from subunit c*, which includes its predicted HLH motif, reduced the apparent affinity of the eIF3 octameric core for the IRES over 100-fold compared with wild-type octamer (Figure 2A), indicating that amino acids 302–343 in subunit c* also contribute to HCV IRES binding by the eIF3 octamer. Importantly, truncations of the predicted HLH motif in eIF3a, or of both HLH motifs (Figure 1B), did not interfere with octamer assembly (Supplementary Figure S3A). Similar binding results were obtained with the HCV IRES IIIabc domain RNA (Supplementary Figure S3B). Taken together, these results indicate that both predicted HLH motifs in eIF3 subunits a and c directly bind the IIIabc domain in the HCV IRES.

We next sought to identify the specific amino acids in eIF3 subunits a and c that are critical for eIF3 binding to the HCV IRES RNA. Both HLH motifs in eIF3 subunits a and c are rich in arginines and lysines in the predicted loop region (Figure 1B). Interestingly, mutations of amino acids 340–343 in subunit c* from RGKK to NGEE or of amino acids 36–39 in subunit a* from KSKK to NSEE, neither of which affected complex assembly (Supplementary Figure S3A) effectively mimicked the reduced affinity of the N-terminal truncations for HCV IRES RNA described above. This was true in the context of fully assembled eIF3 octamer (Figure 2B) and purified c* monomer or a*c* dimer (Figure 2C). Similar results were observed in binding experiments with the HCV IRES IIIabc domain RNA (Supplementary Figure S3C).

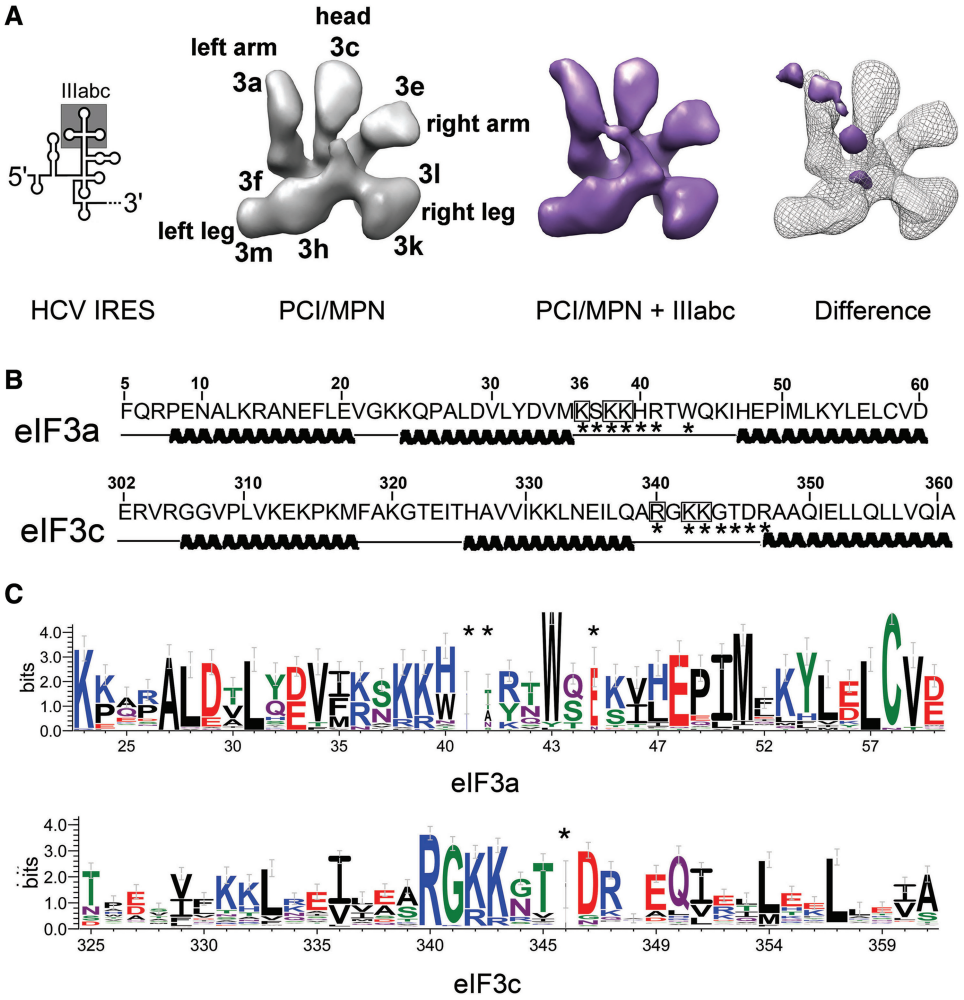

Figure 1. Cryo-EM reconstructions of eIF3 8-mer in its apo and HCV IRES IIIabc-bound form, and sequence analyses of eIF3 subunits a* and c*. (**A**) 3D reconstruction of the eIF3 8-mer (in gray) compared with the 8-mer/IIIabc complex (in purple) and difference map (solid purple positive density at a threshold of 5 sigma on a mesh representation of the apo-8-mer). The secondary structure of the HCV IRES and IIIabc region are shown to the left. Anthropomorphic features of eIF3, as indicated in (14), are also indicated. (**B**) Sequence analyses of the N-termini of subunits a* and c* with BindN (29) and Phyre^2 (30). Amino acids predicted to be RNA-binding motifs (stars) and those mutated in the present study (boxed) are shown. (**C**) Sequence alignment logo (31) for the predicted HLH motif in eIF3 subunit a in metazoan eIF3s, and logo for the predicted HLH motif in eIF3 subunit c in all eukaryotic eIF3s. Asterisks indicate insertions relative to the human sequence. Numbering is also according to the human sequence.

Thus, the loop residues of both HLH motifs in eIF3 subunits a and c are critical for eIF3 binding to the HCV IRES RNA.

eIF3a is the dominant subunit interacting with the HCV IRES

Subunits eIF3b and eIF3d have also been proposed to be involved in eIF3 binding to the HCV IRES (10,17). To test the contribution of subunits beyond eIF3a and eIF3c to HCV IRES binding, we reconstituted eIF3 complexes containing the octameric core plus eIF3d (9-mer), plus eIF3d and eIF3b (10-mer) or with all eIF3 subunits except eIF3j (12-mer) (Supplementary Materials and Methods). As observed for octamer assembly, mutations in subunits a* and c* did not interfere with eIF3 9-12 subunit reconstitutions (Supplementary Figure S3A). Comparisons of the eIF3 octamer with 9-mer and 10-mer assemblies, each incorporating the above mutations in the HLH motifs in subunits a* and/or c*, revealed that subunits b and d contribute only modestly to HCV IRES binding (Figure 2B). In the context of 12-mer eIF3 complexes (octamer plus subunits b, d, g and i), mutations in the c* HLH motif weakened HCV IRES binding modestly, whereas mutations in the HLH domain of subunit a* reduced the apparent affinity of the 12-mer for the IRES by ~20-fold (16) (Figure 2D). These data therefore indicate that subunits a, b, c and d all contribute to eIF3 binding to the HCV IRES, with subunit eIF3a playing the dominant role through its HLH motif.

To identify the regions within the HCV IRES that contact the predicted HLH motifs in eIF3 subunits a* and c*, we used SHAPE (selective 2′-hydroxyl acylation analyzed by primer extension) chemistry to analyze the flexibility of each nucleotide in the HCV IRES in the absence and presence of wild-type eIF3 octamer, 10-mer

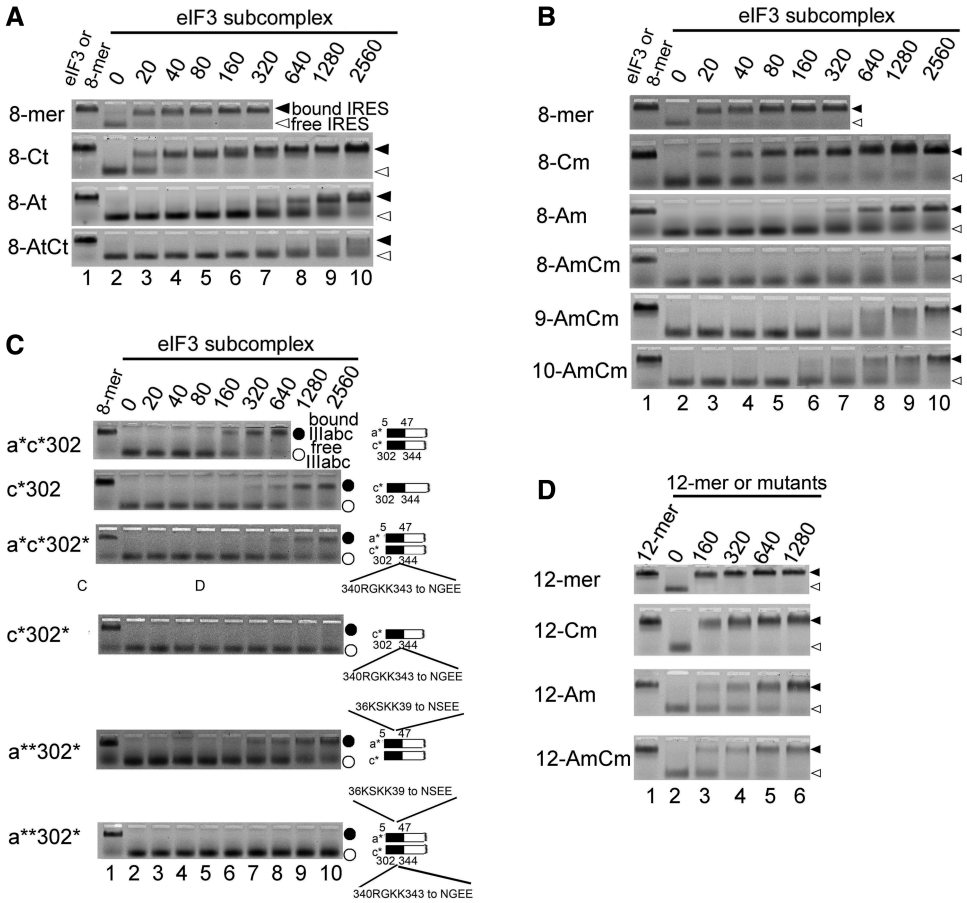

Figure 2. Determination of the critical residues in eIF3 subunits a and c subunits important for interaction with the HCV IRES. (**A**) Native agarose gel showing binding of the eIF3 8-mer and its truncated versions (8-At, 8-Ct and 8-AtCt) to the full-length HCV IRES. (**B**) Native agarose gel showing binding to the full-length HCV IRES of the eIF3 8-mer, 8-mer with mutations in the subunit c HLH motif and/or 8-mer with mutations in the subunit a HLH motif (8-Am, 8-Cm and 8-AmCm, respectively), the 9-mer double-mutant (9-AmCm) and the 10-mer double-mutant (10-AmCm). (**C**) Native agarose gel showing binding of the eIF3 subunit c* and a*c* dimer to the HCV IRES IIIabc domain. The schemes of c*302 and its mutants and a*c*302 and its mutants are drawn on the right side of the corresponding panels. (**D**) Native agarose gel showing binding of wild-type and mutant eIF3 12-mer (12-Am, 12-Cm and 12-AmCm) to the full-length HCV IRES. Concentrations of native human eIF3, 8-mer and 8-mer mutants, 9-mer and 10-mer mutants, 12-mer and 12-mer mutants are listed in nM. Lane 1 shows HCV IRES RNA or IIIabc binding to native eIF3 or 8-mer as a control. Fluorescent full-length IRES was used at 20 nM in concentration, and the reactions were carried out in the presence of 2 μM tRNA to prevent nonspecific binding.

or with mutations in the predicted HLH motif of subunit c* (19) (Supplementary Materials and Methods). The eIF3 octamer or 10-subunit complex strongly protected the HCV IRES IIIb stem-loop from SHAPE reactivity (Figure 3), consistent with the IIIb region serving as the main binding site for eIF3 (9). The eIF3 octamer with mutations in the HLH motif of subunit eIF3c, which slightly reduced IRES binding (Figure 3), also protected the IIIb stem-loop from SHAPE reactivity, albeit less strongly (Figure 3). Together with the mutational analysis above (Figure 2), these results indicate that the HLH motif of subunit eIF3a makes the most extensive contacts with the HCV IRES by binding the IRES IIIb stem loop. Subunit eIF3c may augment this primary interaction rather than contacting an entirely separate region of the IRES, whereas subunits eIF3b and eIF3d may contribute to additional contacts near the lower portions of domain III and the pseudoknot regions of the IRES (Figure 3).

Mutations in eIF3a and eIF3c impair the formation of HCV IRES-dependent translation initiation complexes

The Proteasome, COP9, eIF3/Mpr1-Pad1 N terminal (PCI/MPN) octameric core of eIF3 binds the 40S ribosomal subunit with only 2–3-fold weaker affinity compared with native eIF3 (16). Considering the importance of the N-termini of eIF3 subunits a* and c* for HCV IRES binding, as well as their proximity to the 40S subunit (14), we tested whether mutations in the HLH motifs in subunits a and c affect the interaction of eIF3 with the 40S ribosomal subunit. Remarkably, eIF3 octameric core complexes with mutations in the HLH motifs bound the 40S ribosomal subunit with severely reduced affinity (Supplementary Figure S4). The addition of subunits b, d, g and i restored 40S ribosomal subunit binding of eIF3 complexes with mutations in the HLH motifs to some degree (Figure 4). These results indicate that the HLH motifs in eIF3a and eIF3c are important for eIF3 binding to the 40S ribosomal subunit, as well as to the HCV IRES.

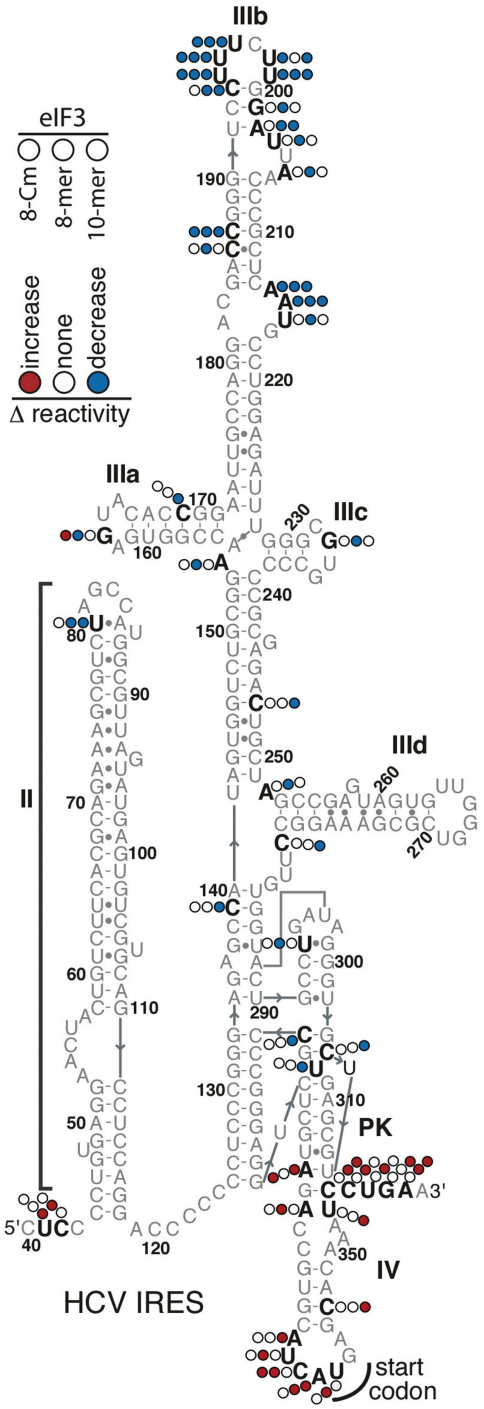

Figure 3. Identification of the eIF3 binding sites in the HCV IRES. SHAPE reactivity differences mapped onto the secondary structure of the IRES IIIabc domain in the presence of eIF3 8-mer mutated in the subunit c HLH motif (8-Cm), 8-mer or 10-mer, indicated from left to right by colored circles. Nucleotides in the HCV IRES that show greater (red) or reduced (blue) SHAPE reactivity in the presence of the eIF3 subcomplexes are indicated.

Because mutations in the HLH motifs of eIF3 subunits a* and c* impair the association of eIF3 with the HCV IRES and 40S ribosomal subunit individually, we tested whether the mutations would impair the formation of preinitiation complexes in HCV IRES-dependent

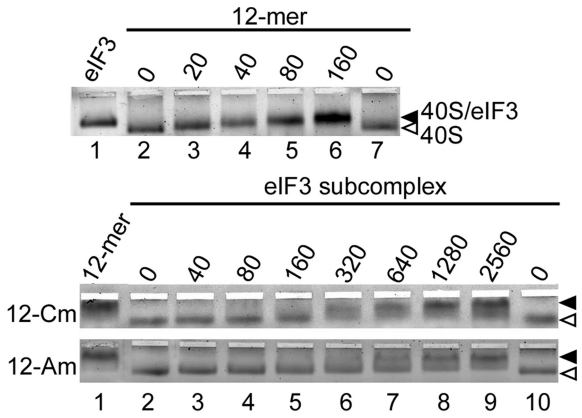

Figure 4. Binding of wild-type and mutant eIF3 complexes to the 40S ribosomal subunit. Native agarose gel showing binding of the eIF3 wild-type and mutant 12-mer eIF3 to the 40S ribosomal subunit, monitored by UV absorbance of the 40S subunit rRNA. The nanomolar concentrations of the eIF3 complexes are indicated. The 40S ribosomal subunit was used at a concentration of 10 nM. The binding of the 40S subunit to natively purified human eIF3 or 12-mer is shown as a control (lane 1).

translation. We first tested the formation of preinitiation complexes on the 40S ribosomal subunit in the presence of reconstituted and glutathione S-transferase (GST)-tagged eIF3 or its mutants in rabbit reticulocyte lysates (RRLs) programmed with an HCV IRES-containing model mRNA (Supplementary Materials and Methods). In RRL reactions with 2 mM of the non-hydrolyzable GTP analogue GMPPNP to stall preinitiation complex formation, wild-type reconstituted eIF3 formed preinitiation complexes containing the 40S ribosomal subunit, eIF2/Met-tRNA$_i$ and the HCV IRES-containing mRNA (Figure 5A and B and Supplementary Figure S5B) (16). Whereas mutations in the HLH motif of eIF3c only slightly impaired preinitiation complex formation (Figure 5B, fractions 2 and 3), mutations in the HLH motif of eIF3a drastically reduced the formation of preinitiation complexes containing the HCV IRES mRNA and eIF2/Met-tRNA$_i$ (Figure 5B).

We also tested the formation of 80S ribosome complexes stalled in the presence of cycloheximide (32) with wild-type reconstituted eIF3 and the above mutant forms in RRL programmed with the HCV IRES-containing model mRNA (Figure 5C and D, and Supplementary Figure S5C). In RRL reactions containing cycloheximide to stall translation after formation of programmed 80S ribosomes (32), mutation of the HLH motif in eIF3c did not impact the formation of 48S preinitiation complexes (Figure 5D, fractions 2 and 3), but decreased the formation of functional 80S complexes containing initiator tRNA (Figure 5D, fraction 4). Interestingly, defects in the formation of programmed 80S ribosomes due to the mutations in eIF3c* correlated with defects in the association of translation initiation factor eIF5B with preinitiation complexes (Figure 5D). In eIF2-mediated translation initiation, eIF5B is generally required after start codon recognition and eIF2–GDP release, in a second GTP-dependent step that leads to 60S subunit joining (33,34). Consistent with the experiments with

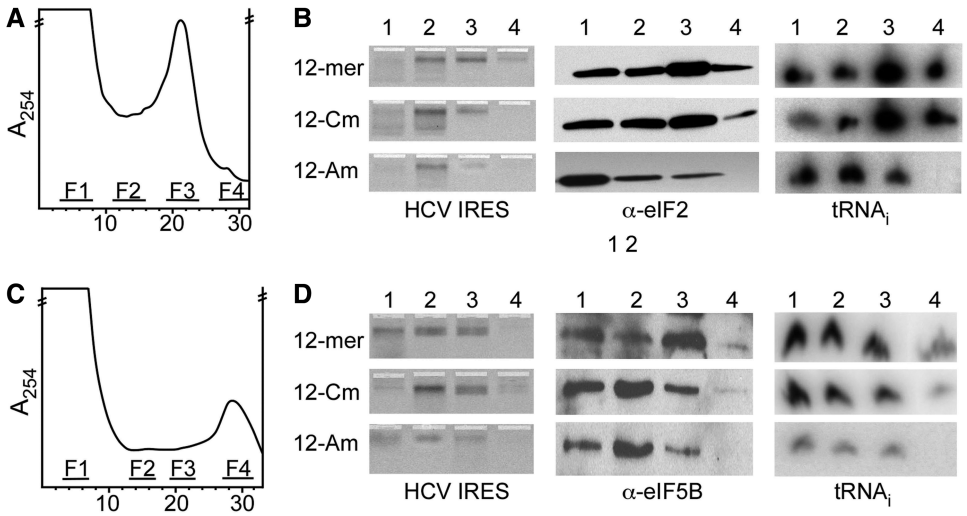

Figure 5. Preinitiation complex formation in the presence of GST-tagged recombinant eIF3 dodecamers. (**A**) Sucrose gradient profile of RRL translation reaction stalled with GMPPNP and programmed with fluorescently labeled HCV IRES-containing mRNA in the presence of wild-type eIF3 dodecamer. The top of the gradient is to the left, and the absorbance at 254 nm is shown. Fractions pooled for GST affinity purification and analysis are marked 1–4. Gradients for 12-Cm and 12-Am reactions look essentially identical to that for wild-type 12-mer, due to the presence of endogenous eIF3 in the in vitro translation (IVT) reaction. (**B**) Analyses of GST affinity-purified products in the presence of GMPPNP. Native agarose gel of fluorescently labeled HCV IRES, western blotting of eIF2α and northern blotting of $tRNA_i$ from pooled fractions 1–4 in panel (A). (**C**) Sucrose gradient profile of an RRL translation reaction as in (A), but stalled with cycloheximide instead of GMPPNP. (**D**) Analyses of GST affinity-purified products in the presence of cycloheximide. Native agarose gel of fluorescently labeled HCV IRES, western blotting of eIF5B and northern blotting of $tRNA_i$, from pooled fractions 1–4 in panel (C). Gradients for 12-Cm and 12-Am reactions look essentially identical to that for wild-type 12-mer, due to the presence of endogenous eIF3 in the IVT reaction. Additional western blots of GST and eIF2 and northern blots of 18S and 28S rRNA for the GMPPNP- and cycloheximide-stalled reactions are included in Supplementary Figure S5.

GMPPNP, mutation of the HLH motif in eIF3a resulted in even more severe defects, eliminating the ability of reconstituted eIF3 to mediate Met-$tRNA_i$ loading into 80S complexes (Figure 5D). Taken together, these results indicate that the HLH motif in eIF3a contributes to eIF2-dependent Met-$tRNA_i$ binding to preinitiation complexes, whereas the HLH motif in eIF3c is important for eIF5B association with preinitiation complexes.

DISCUSSION

Although eIF3 is essential for the function of the HCV IRES in translation initiation (12,35,36) and binds tightly to the HCV IRES in isolation (9,10), the molecular mechanism by which it stimulates initiation from HCV IRES has not been clear. Using cryo-EM data as a guide, we were able to predict the location of HLH RNA-binding motifs in eIF3 subunits a and c, and to show that these HLH motifs make direct contacts with the HCV IRES. Furthermore, these HLH motifs are important for eIF3 binding to the 40S ribosomal subunit. The contacts between the HLH motifs to the HCV IRES and 40S ribosomal subunit are augmented by contributions from subunits b and d, consistent with previous cross-linking results (10,17).

Based on the experiments in translation extracts, the HLH motif in eIF3a serves as a lynchpin in assembling translation initiation complexes on the HCV IRES. The HLH motif in eIF3a contributes to early steps of HCV IRES-mediated translation initiation dependent on eIF2, before start codon selection, whereas the eIF3c HLH motif is important for later events dependent on eIF5B, after start codon selection but before 60S subunit joining (Figure 6). Intriguingly, the HLH motif in eIF3a is highly conserved across metazoans and is present in most eukaryotes with available genome sequences (Figure 1C, Supplementary Figure S2D), suggesting that this motif may play a role in loading of the eIF2–GTP–Met-$tRNA_i$ ternary complex into translation preinitiation complexes on cellular mRNAs as well as the HCV genomic RNA. The HLH motif in eIF3c is highly conserved in all eukaryotes (Figure 1C), implying that its role in eIF5B exchange with eIF2 after start codon selection to catalyze 60S ribosomal subunit joining (33,37) may be a nearly universal feature of eukaryotic translation initiation. Interestingly, the conformation of the eIF3 octameric core closely resembles the proteasome lid subcomplex once it is bound to the 26S proteasome holoenzyme, which causes the N-terminus of Rpn5 to adopt an extended conformation, similar to the conformation seen here for eIF3a (38). The a* and c* arms are the most mobile elements in the eIF3 core, and correspond to the eIF3 regions in closest proximity to the mRNA binding cleft of the 40S subunit (14,28). The flexibility of these arms in eIF3 may be important for their function in translation initiation complex assembly. Based on its location in eIF3, the eIF3c HLH motif would be positioned near the head domain of the 40S ribosomal subunit (14,28). Contacts between the eIF3c HLH domain and the head of the 40S subunit, which is thought to adopt a closed conformation after start codon selection (11,39), may serve to stimulate eIF2 exchange with eIF5B after start codon recognition (40).

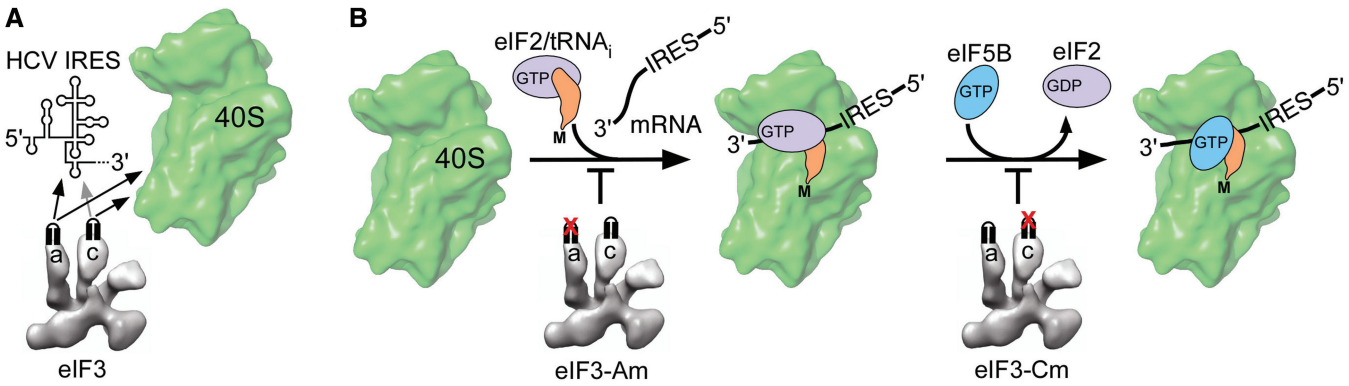

Figure 6. The roles of the HLH motifs in eIF3 subunits a and c subunits in translation initiation complex formation. (**A**) Mutations in the HLH motif of eIF3a greatly weaken eIF3 binding to the HCV IRES and 40S ribosomal subunit, whereas mutations in the HLH motif of eIF3c primarily affect eIF3 binding to the 40S ribosomal subunit. (**B**) Mutations in the HLH motif of eIF3a disrupt eIF2-mediated Met-tRNA$_i$ loading into preinitiation complexes, whereas mutations in the eIF3c HLH motif impair eIF5B exchange with eIF2 after start codon recognition.

The present experiments identified a surprisingly localized contact between an HLH motif in eIF3a and the IIIb stem-loop of the HCV IRES RNA that controls the efficiency of IRES-mediated preinitiation complex assembly and functional 80S ribosome formation. The local nature of this contact could serve as a new target for the development of small molecule therapeutics to inhibit HCV IRES-mediated translation initiation. In conditions of cellular stress when active eIF2 pools are depleted, the eIF3c HLH motif may also play an important role in an alternative eIF5B-mediated translation initiation pathway using the HCV IRES (36). In this alternative pathway, translation initiation occurs without the requirement for eIF2. It will be interesting in future experiments to investigate how these two HLH motifs in eIF3 contribute to regulating translation initiation on cellular mRNAs in different physiological contexts.

DATABASE

The Cryo-EM map of the eIF3 PCI/MPN octameric complex and maps used to generate the difference map with the IIIabc RNA have been deposited in the Electron Microscopy Data Bank under accession codes EMD-2166, EMD-2198 and EMD-2199.

SUPPLEMENTARY DATA

Supplementary Data are available at NAR Online: Supplementary Tables 1 and 2, Supplementary Figures 1–5, Supplementary Materials and Methods and Supplementary References [41–52].

ACKNOWLEDGEMENTS

The authors thank G. Lander for invaluable technical help, P. Grob and T. Houweling for electron microscopy and computational support, respectively, and D. Smith for helpful discussions on the manuscript.

FUNDING

National Institutes of Health (NIH) [R56-AI095687 to J.H.D.C.; P50-GM102706 to J.A.D. and J.H.D.C.]; Spanish Ministry of Education through the Programa Nacional de Movilidad de Recursos Humanos del Plan Nacional de I-D+i 2008-2011 (to E.A.-P.). J.A.D. and E.N. are Howard Hughes Medical Institute Investigators. Funding for open access charge: NIH [P50-GM102706].

Conflict of interest statement. None declared.

REFERENCES

1. Hinnebusch,A.G. (2011) Molecular mechanism of scanning and start codon selection in eukaryotes. *Microbiol. Mol. Biol. Rev.*, **75**, 434–467, first page of table of contents.
2. Hinnebusch,A.G. and Lorsch,J.R. (2012) The mechanism of eukaryotic translation initiation: new insights and challenges. *Cold Spring Harb. Perspect. Biol.*, **4**, pii: a011544.
3. Jackson,R.J., Hellen,C.U. and Pestova,T.V. (2010) The mechanism of eukaryotic translation initiation and principles of its regulation. *Nat. Rev. Mol. Cell Biol.*, **11**, 113–127.
4. Fraser,C.S. and Doudna,J.A. (2007) Structural and mechanistic insights into hepatitis C viral translation initiation. *Nat. Rev. Microbiol.*, **5**, 29–38.
5. Sokabe,M., Fraser,C.S. and Hershey,J.W. (2012) The human translation initiation multi-factor complex promotes methionyl-tRNAi binding to the 40S ribosomal subunit. *Nucleic Acids Res.*, **40**, 905–913.
6. Pisarev,A.V., Kolupaeva,V.G., Yusupov,M.M., Hellen,C.U. and Pestova,T.V. (2008) Ribosomal position and contacts of mRNA in eukaryotic translation initiation complexes. *EMBO J.*, **27**, 1609–1621.
7. Silvera,D., Formenti,S.C. and Schneider,R.J. (2010) Translational control in cancer. *Nat. Rev. Cancer*, **10**, 254–266.
8. Kieft,J.S., Zhou,K., Jubin,R., Murray,M.G., Lau,J.Y. and Doudna,J.A. (1999) The hepatitis C virus internal ribosome entry site adopts an ion-dependent tertiary fold. *J. Mol. Biol.*, **292**, 513–529.
9. Kieft,J.S., Zhou,K., Jubin,R. and Doudna,J.A. (2001) Mechanism of ribosome recruitment by hepatitis C IRES RNA. *RNA*, **7**, 194–206.
10. Sizova,D.V., Kolupaeva,V.G., Pestova,T.V., Shatsky,I.N. and Hellen,C.U. (1998) Specific interaction of eukaryotic translation initiation factor 3 with the 5' nontranslated regions of hepatitis C virus and classical swine fever virus RNAs. *J. Virol.*, **72**, 4775–4782.

11. Spahn,C.M., Kieft,J.S., Grassucci,R.A., Penczek,P.A., Zhou,K., Doudna,J.A. and Frank,J. (2001) Hepatitis C virus IRES RNA-induced changes in the conformation of the 40s ribosomal subunit. *Science*, **291**, 1959–1962.
12. Pestova,T.V., Shatsky,I.N., Fletcher,S.P., Jackson,R.J. and Hellen,C.U. (1998) A prokaryotic-like mode of cytoplasmic eukaryotic ribosome binding to the initiation codon during internal translation initiation of hepatitis C and classical swine fever virus RNAs. *Genes Dev.*, **12**, 67–83.
13. Tsukiyama-Kohara,K., Iizuka,N., Kohara,M. and Nomoto,A. (1992) Internal ribosome entry site within hepatitis C virus RNA. *J. Virol.*, **66**, 1476–1483.
14. Siridechadilok,B., Fraser,C.S., Hall,R.J., Doudna,J.A. and Nogales,E. (2005) Structural roles for human translation factor eIF3 in initiation of protein synthesis. *Science*, **310**, 1513–1515.
15. Damoc,E., Fraser,C.S., Zhou,M., Videler,H., Mayeur,G.L., Hershey,J.W., Doudna,J.A., Robinson,C.V. and Leary,J.A. (2007) Structural characterization of the human eukaryotic initiation factor 3 protein complex by mass spectrometry. *Mol. Cell. Proteomics*, **6**, 1135–1146.
16. Sun,C., Todorovic,A., Querol-Audi,J., Bai,Y., Villa,N., Snyder,M., Ashchyan,J., Lewis,C.S., Hartland,A., Gradia,S. *et al.* (2011) Functional reconstitution of human eukaryotic translation initiation factor 3 (eIF3). *Proc. Natl Acad. Sci. USA*, **108**, 20473–20478.
17. Buratti,E., Tisminetzky,S., Zotti,M. and Baralle,F.E. (1998) Functional analysis of the interaction between HCV 5'UTR and putative subunits of eukaryotic translation initiation factor eIF3. *Nucleic Acids Res.*, **26**, 3179–3187.
18. Cai,Q., Todorovic,A., Andaya,A., Gao,J., Leary,J.A. and Cate,J.H. (2010) Distinct regions of human eIF3 are sufficient for binding to the HCV IRES and the 40S ribosomal subunit. *J. Mol. Biol.*, **403**, 185–196.
19. Mortimer,S.A. and Weeks,K.M. (2009) Time-resolved RNA SHAPE chemistry: quantitative RNA structure analysis in one-second snapshots and at single-nucleotide resolution. *Nat. Protoc.*, **4**, 1413–1421.
20. Mortimer,S.A. and Weeks,K.M. (2007) A fast-acting reagent for accurate analysis of RNA secondary and tertiary structure by SHAPE chemistry. *J. Am. Chem. Soc.*, **129**, 4144–4145.
21. Barbu,V. and Dautry,F. (1989) Northern blot normalization with a 28S rRNA oligonucleotide probe. *Nucleic Acids Res.*, **17**, 7115.
22. Lander,G.C., Stagg,S.M., Voss,N.R., Cheng,A., Fellmann,D., Pulokas,J., Yoshioka,C., Irving,C., Mulder,A., Lau,P.W. *et al.* (2009) Appion: an integrated, database-driven pipeline to facilitate EM image processing. *J. Struct. Biol.*, **166**, 95–102.
23. van Heel,M., Harauz,G., Orlova,E.V., Schmidt,R. and Schatz,M. (1996) A new generation of the IMAGIC image processing system. *J. Struct. Biol.*, **116**, 17–24.
24. Ludtke,S.J., Baldwin,P.R. and Chiu,W. (1999) EMAN: semiautomated software for high-resolution single-particle reconstructions. *J. Struct. Biol.*, **128**, 82–97.
25. Tang,G., Peng,L., Baldwin,P.R., Mann,D.S., Jiang,W., Rees,I. and Ludtke,S.J. (2007) EMAN2: an extensible image processing suite for electron microscopy. *J. Struct. Biol.*, **157**, 38–46.
26. Scheres,S.H., Nunez-Ramirez,R., Gomez-Llorente,Y., San Martin,C., Eggermont,P.P. and Carazo,J.M. (2007) Modeling experimental image formation for likelihood-based classification of electron microscopy data. *Structure*, **15**, 1167–1177.
27. Sorzano,C.O., Marabini,R., Velazquez-Muriel,J., Bilbao-Castro,J.R., Scheres,S.H., Carazo,J.M. and Pascual-Montano,A. (2004) XMIPP: a new generation of an open-source image processing package for electron microscopy. *J. Struct. Biol.*, **148**, 194–204.
28. Querol-Audi,J., Sun,C., Vogan,M.J., Smith,M.D., Gu,Y., Cate,J.H. and Nogales,E. (2013) Architecture of human translation initiation factor 3. *Structure*, **21**, 920–928.
29. Wang,L. and Brown,S.J. (2006) BindN: a web-based tool for efficient prediction of DNA and RNA binding sites in amino acid sequences. *Nucleic Acids Res.*, **34**, W243–W248.
30. Kelley,L.A. and Sternberg,M.J. (2009) Protein structure prediction on the Web: a case study using the Phyre server. *Nat. Protoc.*, **4**, 363–371.
31. Crooks,G.E., Hon,G., Chandonia,J.M. and Brenner,S.E. (2004) WebLogo: a sequence logo generator. *Genome Res.*, **14**, 1188–1190.
32. Dmitriev,S.E., Pisarev,A.V., Rubtsova,M.P., Dunaevsky,Y.E. and Shatsky,I.N. (2003) Conversion of 48S translation preinitiation complexes into 80S initiation complexes as revealed by toeprinting. *FEBS Lett.*, **533**, 99–104.
33. Pestova,T.V., Lomakin,I.B., Lee,J.H., Choi,S.K., Dever,T.E. and Hellen,C.U. (2000) The joining of ribosomal subunits in eukaryotes requires eIF5B. *Nature*, **403**, 332–335.
34. Lee,J.H., Pestova,T.V., Shin,B.S., Cao,C., Choi,S.K. and Dever,T.E. (2002) Initiation factor eIF5B catalyzes second GTP-dependent step in eukaryotic translation initiation. *Proc. Natl Acad. Sci. USA*, **99**, 16689–16694.
35. Pestova,T.V. and Kolupaeva,V.G. (2002) The roles of individual eukaryotic translation initiation factors in ribosomal scanning and initiation codon selection. *Genes Dev.*, **16**, 2906–2922.
36. Terenin,I.M., Dmitriev,S.E., Andreev,D.E. and Shatsky,I.N. (2008) Eukaryotic translation initiation machinery can operate in a bacterial-like mode without eIF2. *Nat. Struct. Mol. Biol.*, **15**, 836–841.
37. Shin,B.S., Maag,D., Roll-Mecak,A., Arefin,M.S., Burley,S.K., Lorsch,J.R. and Dever,T.E. (2002) Uncoupling of initiation factor eIF5B/IF2 GTPase and translational activities by mutations that lower ribosome affinity. *Cell*, **111**, 1015–1025.
38. Lander,G.C., Estrin,E., Matyskiela,M.E., Bashore,C., Nogales,E. and Martin,A. (2012) Complete subunit architecture of the proteasome regulatory particle. *Nature*, **482**, 186–191.
39. Passmore,L.A., Schmeing,T.M., Maag,D., Applefield,D.J., Acker,M.G., Algire,M.A., Lorsch,J.R. and Ramakrishnan,V. (2007) The eukaryotic translation initiation factors eIF1 and eIF1A induce an open conformation of the 40S ribosome. *Mol. Cell*, **26**, 41–50.
40. Locker,N., Easton,L.E. and Lukavsky,P.J. (2007) HCV and CSFV IRES domain II mediate eIF2 release during 80S ribosome assembly. *EMBO J.*, **26**, 795–805.
41. Valasek,L., Mathew,A.A., Shin,B.S., Nielsen,K.H., Szamecz,B. and Hinnebusch,A.G. (2003) The yeast eIF3 subunits TIF32/a, NIP1/c, and eIF5 make critical connections with the 40S ribosome *in vivo*. *Genes Dev.*, **17**, 786–799.
42. Altschul,S.F., Madden,T.L., Schaffer,A.A., Zhang,J., Zhang,Z., Miller,W. and Lipman,D.J. (1997) Gapped BLAST and PSI-BLAST: a new generation of protein database search programs. *Nucleic Acids Res.*, **25**, 3389–3402.
43. Punta,M., Coggill,P.C., Eberhardt,R.Y., Mistry,J., Tate,J., Boursnell,C., Pang,N., Forslund,K., Ceric,G., Clements,J. *et al.* (2012) The Pfam protein families database. *Nucleic Acids Res.*, **40**, D290–D301.
44. Papadopoulos,J.S. and Agarwala,R. (2007) COBALT: constraint-based alignment tool for multiple protein sequences. *Bioinformatics*, **23**, 1073–1079.
45. Di Tommaso,P., Moretti,S., Xenarios,I., Orobitg,M., Montanyola,A., Chang,J.M., Taly,J.F. and Notredame,C. (2011) T-Coffee: a web server for the multiple sequence alignment of protein and RNA sequences using structural information and homology extension. *Nucleic Acids Res.*, **39**, W13–W17.
46. Berry,K.E., Waghray,S., Mortimer,S.A., Bai,Y. and Doudna,J.A. (2011) Crystal structure of the HCV IRES central domain reveals strategy for start-codon positioning. *Structure*, **19**, 1456–1466.
47. Vasa,S.M., Guex,N., Wilkinson,K.A., Weeks,K.M. and Giddings,M.C. (2008) ShapeFinder: a software system for high-throughput quantitative analysis of nucleic acid reactivity information resolved by capillary electrophoresis. *RNA*, **14**, 1979–1990.
48. Suloway,C., Pulokas,J., Fellmann,D., Cheng,A., Guerra,F., Quispe,J., Stagg,S., Potter,C.S. and Carragher,B. (2005) Automated molecular microscopy: the new Leginon system. *J. Struct. Biol.*, **151**, 41–60.

49. Voss,N.R., Yoshioka,C.K., Radermacher,M., Potter,C.S. and Carragher,B. (2009) DoG Picker and TiltPicker: software tools to facilitate particle selection in single particle electron microscopy. *J. Struct. Biol.*, **166**, 205–213.
50. Mindell,J.A. and Grigorieff,N. (2003) Accurate determination of local defocus and specimen tilt in electron microscopy. *J. Struct. Biol.*, **142**, 334–347.
51. Scheres,S.H., Nunez-Ramirez,R., Sorzano,C.O., Carazo,J.M. and Marabini,R. (2008) Image processing for electron microscopy single-particle analysis using XMIPP. *Nat. Protoc.*, **3**, 977–990.
52. Scheres,S.H., Gao,H., Valle,M., Herman,G.T., Eggermont,P.P., Frank,J. and Carazo,J.M. (2007) Disentangling conformational states of macromolecules in 3D-EM through likelihood optimization. *Nat. Methods*, **4**, 27–29.